ONE-DIMENSIONAL SHORT-RANGE NEAREST-NEIGHBOR INTERACTION AND ITS NONLINEAR DIFFUSION LIMIT

M Fischer, L Kanzler, C Schmeiser

ONE-DIMENSIONAL SHORT-RANGE NEAREST-NEIGHBOR INTERACTION AND ITS NONLINEAR DIFFUSION LIMIT

M. FISCHER, L. KANZLER, C. SCHMEISER

Abstract

Repulsion between individuals within a finite radius is encountered in numerous applications, including cell exclusion, i.e. an overlap of cells to be avoided, bird flocks, or microscopic pedestrian models. We define such individual based particle dynamics in one spatial dimension with minimal assumptions of the repulsion force f and prove their characteristic properties. Moreover, we are able to perform a rigorous limit from the microscopic- to the macroscopic scale, where we could recover the finite interaction radius as a density threshold. Specific choices for the repulsion force f lead to well known nonlinear diffusion equations on the macroscopic scale, as e.g. the porous medium equation. At both scaling levels numerical simulations are presented and compared to underline the analytical results. We discuss the possible applications of this new diffusion term.

Keywords: agent-based models, repulsive force, cell-exclusion, nonlinear diffusion limit, porous medium equation

Mathematics subject classification: 82C22, 35R37, 35K55, 92C15

1. Introduction

We consider a chain of particles keeping their order along a straight line and interacting with their neighbors by distance dependent repulsive forces, which vanish above an equilibrium distance. For a finite number of such particles the distance between the first and the last particle will remain finite for all time. Our goal is to derive a macroscopic continuum model sharing this property, i.e. for an initial particle density with bounded support there should be a finite upper bound for the length of the support at later times. Such a model, in the form of a nonlinear diffusion equation, will be derived from the particle model by a continuum limit. The macroscopic model is diffusive since we choose a friction dominated (overdamped) microscopic model, being motivated by the dynamics of bacterial colonies living in viscous environments.

Repulsive effects with a finite radius are often used in microscopic particle systems and their corresponding kinetic and macroscopic models. In flocking models, most important the Cucker-Smale- and the Vicsek-model, see [12, 42], they appear as part of an interaction between attraction and repulsion. Examples occur in the modelling of collective behaviour within sheep-herds [32], fish schools [10] and bird flocks [9]. In our setting, only neighbouring particles interact, therefore we have a mixture between a metric interaction radius and a topological one as used in [4] or [20] in a kinetic context. A deterministic, Lagrangian many-particle system was also investigated in [13].

Repulsion forces between individuals is also highly relevant in modelling size exclusion effects. On the microscopic level, this has been studied for the pattern formation in bacterial colonies [14, 15, 44]. In general, this new term of size exclusion is a macroscopic

alternative to models based on e.g. cellular automata, compare [35], or microscopic asymmetric exclusion process, see [6], in which size exclusion has no influence on the diffusive term, typically a linear diffusive-term is derived.

This diffusive term can be microscopically interpreted as particles trying to reach a desired density. The desired density is similar to the desired velocity, an important topic in pedestrian dynamics, see [1, 19], gaining new focus in the context of social distancing [26], and cannot be calibrated in other macroscopic models, see [19].

On a macroscopic level this diffusion on a compact support leads to a moving boundary problem. It is closely related to the Stefan-problem, see classical books [27, 34]. Analytically exact solutions are an ongoing topic, see [11, 18] and also numerically challenges occur e.g. also in cancer research, see [38, 22]. On an agent-based level, cancer growth was investigated in [29].

Rigorous limits from microscopic to macroscopic scales can serve to extend the theory of existence of solutions at the PDE level, see [13]. For e.g. the continuous version of the Vicsek-model a rigorous limit to a PDE was performed in [5], transferring regularity results to the macroscopic level. A bounded total variation is a common tool in numerical analysis to show convergence of a discretisation against the solution of a model, see [3, 21, 31, 39].

The modelled repulsion can also be seen as a cut-off potential. On a microscopic level this is often used for better computational speed and e.g. steadier movement of pedestrians as in the optimal-step-model, see [36].

This work is structured as follows. In Section 2 the microscopic model in the form of an ODE system is formulated and its characteristic properties are derived. Section 3 contains a formal derivation of the macroscopic model and a discussion of its qualitative properties. This includes the derivation of a Eulerian formulation of the model, which is originally written in terms of Lagrangian coordinates. Some of the formal results are illustrated by numerical simulations in Section 5. In Section 4 the macroscopic limit is carried out rigorously, providing also a existence of solutions for the continuum model. Finally, some conclusions and an outlook are contained in Section 6.

2. The microscopic model – individual based dynamics

Consider a chain of $N+1$ point particles with time dependent positions $x_i(t) \in \mathbb{R}$, $0 \le i \le N$, such that

$$x_0(t) \le x_2(t) \le \cdots \le x_N(t)\,.$$

Neighboring particles i and $i+1$ interact by a distance dependent repulsive force $F(x_{i+1}-x_i)$, written as $F(r) = F_0 f(r/R)$ in terms of the dimensionless function f, which satisfies

$$f:\,[0,\infty)\to[0,1] \text{ is Lipschitz and nonincreasing,} \quad \operatorname{supp}(f)=[0,1]\,, \tag{1}$$

i.e. there is no interaction between neighbors further apart than the equilibrium distance $R>0$. Balancing these interaction forces with friction against a nonmoving environment (with friction coefficient $\mu>0$) leads to the ODE system

$$\begin{aligned} \mu\dot{x}_0 &= -F\left(x_1-x_0\right)\,,\\ \mu\dot{x}_i &= F\left(x_i-x_{i-1}\right)-F\left(x_{i+1}-x_i\right)\,, \qquad 1\le i\le N-1\,,\\ \mu\dot{x}_N &= F\left(x_N-x_{N-1}\right)\,. \end{aligned} \tag{2}$$

We introduce a nondimensionalization by

$$x \to NRx\,, \qquad t\to N^2\frac{\mu R}{F_0}t\,.$$

This is a diffusive macroscopic rescaling (by the factors N and, respectively, N^2) of the natural microscopic scaling. The scaled system reads

$$\begin{aligned} \dot{x}_0 &= -Nf\left(N(x_1-x_0)\right), \\ \dot{x}_i &= N\left(f\left(N(x_i-x_{i-1})\right)-f\left(N(x_{i+1}-x_i)\right)\right), \qquad 1\le i\le N-1, \\ \dot{x}_N &= Nf\left(N(x_N-x_{N-1})\right). \end{aligned} \tag{3}$$

We shall mostly work with a reformulation in terms of the new unknowns

$$\omega_i := N(x_i-x_{i-1}), \quad 1\le i\le N, \tag{4}$$

satisfying

$$\begin{aligned} \dot{\omega}_1 &= N^2\left[2f\left(\omega_1\right)-f\left(\omega_2\right)\right], \\ \dot{\omega}_i &= N^2\left[2f\left(\omega_i\right)-f\left(\omega_{i-1}\right)-f\left(\omega_{i+1}\right)\right], \quad 2\le i\le N-1, \\ \dot{\omega}_N &= N^2\left[2f\left(\omega_N\right)-f\left(\omega_{N-1}\right)\right]. \end{aligned} \tag{5}$$

This system will be considered subject to initial conditions

$$\omega_i(0)=\omega_{i,0}\ge 0, \qquad 1\le i\le N. \tag{6}$$

We start with stating global existence and boundedness of the solution.

Theorem 1. *Let f satisfy (1). Then there exists a unique global solution $(\omega_1,\dots,\omega_N)\in C^{1,1}\left([0,\infty)\right)^N$ of (5), (6), which satisfies*

$$\omega_{\min} := \min_{1\le j\le N}\omega_{j,0} \le \omega_i(t) \le \max\left\{1, \max_{1\le j\le N}\omega_{j,0}\right\} =: \omega_{\max}, \qquad t\ge 0,\ 1\le i\le N.$$

Proof. Global existence and uniqueness follow from the Lipschitz continuity of f. The upper bound is an obvious consequence of the facts that $f\ge 0$ and $f(\omega_{\max})=0$.

Now assume that $\omega_i(t_0)=\omega_{\min}$ and $\omega_j(t_0)\ge\omega_{\min}$, $1\le j\le N$. In the case $2\le i\le N-1$ we then have

$$\dot{\omega}_i(t_0) = N^2\left[2f\left(\omega_{\min}\right)-f\left(\omega_{i-1}(t_0)\right)-f\left(\omega_{i+1}(t_0)\right)\right]\ge 0,$$

by the monotonicity of f, and similarly for $i=1,N$. □

The following results for the particle positions show that they expand around their center of mass, but not too much.

Theorem 2. *Let $(x_0,\dots,x_N)$ be a solution of (3), satisfying (4), (6). Then*

1) the center of mass

$$\bar{x} := \frac{1}{N+1}\sum_{i=0}^{N} x_i$$

is conserved, i.e. $d\bar{x}/dt=0$,

2) the variance

$$\mathcal{V}_x(t) := \frac{1}{N}\sum_{i=0}^{N}\left(x_i-\bar{x}\right)^2$$

is a nondecreasing function of time, and

3) the distance between the leftmost and the rightmost particle remains bounded:

$$x_N(t)-x_0(t)\le\omega_{\max}, \qquad t\ge 0.$$

Proof. The scalar product of (3) with $(\varphi_0(t), \dots, \varphi_N(t))$ gives, after summation by parts,

$$\sum_{i=0}^{N} \dot{x}_i \varphi_i = \sum_{i=1}^{N} f(\omega_i) N \left(\varphi_i - \varphi_{i-1}\right) . \tag{7}$$

This immediately implies 1) with $\varphi_0 = \cdots = \varphi_N = 1$. The choice $\varphi_i(t) = \frac{2}{N}(x_i(t) - \bar{x})$, $i = 0, \dots, N$, gives

$$\dot{\mathcal{V}}_x(t) = \frac{2}{N} \sum_{i=1}^{N} f(\omega_i)\omega_i \geq 0 ,$$

proving 2). Statement 3) is a consequence of

$$x_N(t) - x_0(t) = \frac{1}{N} \sum_{i=1}^{N} \omega_i(t) ,$$

and of the upper bound in Theorem 1. □

3. The macroscopic model

The continuum model in Lagrangian coordinates: Interpreting the particle index as a discrete Lagrangian variable, the connection to the continuum is made by the definitions

$$\Delta s := \frac{1}{N} , \qquad s_i := i\Delta s , \quad 0 \leq i \leq N ,$$

a discretization of the Lagrangian coordinate $s \in [0, 1]$. Assuming the existence of a function $\omega(s, t)$, such that $\omega_i(t) \approx \omega(s_i, t)$ as $N \to \infty$, the formal limit of the second equation in (5) gives

$$\partial_t \omega = -\partial_s^2 f(\omega) , \qquad 0 < s < 1 , \tag{8}$$

a nonlinear diffusion equation with the diffusivity $-f'(\omega) \geq 0$, which is bounded by the Lipschitz continuity of f. The limits of the first and third equation in (5) lead to

$$f(\omega(0, t)) = f(\omega(1, t)) = 0 , \tag{9}$$

equivalent to

$$\omega \geq 1 , \qquad s = 0, 1 . \tag{10}$$

This looks like incomplete information on the boundary. However, it is sufficient in view of the degenerate diffusivity. If, on the one hand, $\omega > 1$ next to the boundary, then the diffusivity vanishes there, the solution does not change with t, and the boundary condition is satisfied. If, on the other hand $\omega(0+, t) \leq 1$ (or, respectively, $\omega(1-, t) \leq 1$) then the solution needs to take the boundary value 1.

Similarly, the continuum limit of the particle positions $x(s, t)$, satisfying $\partial_s x = \omega$, solves the Neumann type problem

$$\begin{aligned} &\partial_t x = -\partial_s f(\partial_s x) , \qquad 0 < s < 1 , \\ &\partial_s x \geq 1 , \qquad s = 0, 1 . \end{aligned} \tag{11}$$

Eulerian coordinates – the particle density: Our next goal is to write the equation (8) in terms of the Eulerian coordinate x instead of the Lagrangian coordinate s. This produces a *moving boundary problem* posed on the x-interval $[X_0(t), X_1(t)] := [x(0,t), x(1,t)]$. The coordinate transformation can be written as

$$x = X_0(t) + \int_0^s \omega(\sigma, t) d\sigma \,, \tag{12}$$

implying

$$\partial_s \to \omega \partial_x, \quad \partial_t \to \partial_t - \omega \partial_x f(\omega) \partial_x \,,$$

where (11) at $s = 0$ and (8) have been used. Consequently the Eulerian version of (8) reads

$$\partial_t \omega = -\omega^2 \partial_x^2 f(\omega) \,, \qquad X_0 < x < X_1 \,.$$

This is equivalent to the conservation law

$$\partial_t \rho = \partial_x^2 f\left(\frac{1}{\rho}\right) \,, \qquad X_0 < x < X_1 \,, \tag{13}$$

for the macroscopic particle density $\rho := 1/\omega$, which is complemented by the boundary conditions

$$\rho \le 1 \,, \qquad x = X_0, X_1 \,,$$

and by the dynamics of the moving boundaries, determined from (11):

$$\dot{X}_{0,1} = -\frac{1}{\rho} \partial_x f\left(\frac{1}{\rho}\right) \Big|_{x = X_{0,1}} \,. \tag{14}$$

Jump discontinuities: As a consequence of the degeneracy of the diffusivity $D(\rho) := -\rho^{-2} f'(1/\rho)$ for $\rho \le 1$, the nonlinear diffusion equation (13) supports jumps between values $\rho(x_*-, t) = 1$ and $\rho(x_*+, t) < 1$. The velocity of the jump location $x_*(t)$ is given by the *Rankine-Hugoniot condition*

$$\dot{x}_* = \frac{-\partial_x f(1/\rho)|_{x=x_*-}}{1 - \rho|_{x=x_*+}} \,. \tag{15}$$

With the obvious changes also the case $\rho(x_*-, t) < 1$ and $\rho(x_*+, t) = 1$ can be considered. Such jumps typically separate regions where $\rho \ge 1$ from regions where $\rho < 1$. Note that with the natural assumption $\partial_x \rho(x_*(t)-, t) \le 0$, the formula above implies $\dot{x}_* \ge 0$, i.e. the jump moves towards the region of lower density. In the case $\rho(X_{0,1}(t), t) = 1$, the moving boundary equation (14) can be seen as a special case of (15), with ρ continued by zero outside of $[X_0, X_1]$. Otherwise, i.e. when $\rho(X_{0,1}(t), t) < 1$, the boundary does not move.

Special cases: The statements above do not cover the situation of initial data with a smooth transition between $\rho > 1$ and $\rho < 1$. Consider an initial datum $\rho_0(x) = 1 - cx$, $c > 0$, and the choice $f(\omega) = (1 - \omega)_+$. We expect that a discontinuity develops with location $x_*(t)$ starting at $x_*(0) = 0$. Approximating the denumerator on the right hand side of (15) by its value at $t = 0$, we obtain

$$\dot{x}_* \approx \frac{1}{x_*} \,,$$

and therefore $x_\star(t) \approx \sqrt{2t}$ for small t. This behavior with infinite initial velocity also occurs in the Stefan-problem, see e.g. [2, Chapter 1, Example 1]. It can also be seen on a microscopic level in Figure 1a for x_0 and x_N.

Another special case is initial data with $\rho_0 > 1$ in a bounded interval, $\rho_0 = 1$ outside of it, and $f(\omega) = (1/\omega - 1)_+^m$, $m \in \mathbb{R}$. For $m \ge 1$ the shifted density $\rho - 1$ solves the *porous medium equation* with initial data with bounded support, a problem very well studied (see

e.g. [41]). In particular, in that case $\mathrm{supp}(\rho - 1)$ will grow, and the long-time behavior of the solution is given by an explicitly computable self-similar *Barenblatt profile*. For $m \in [0, 1)$ we are in the case where $\rho - 1$ solves the *fast diffusion equation*, which also is well investigated, see e.g. [8]. For $m < 0$ this phenomenon is known as *super-fast diffussion*. For a survey of results regarding these types of nonlinear diffusion we refer the reader to [40]. If the initial data are such that the flux $\partial_x f(1/\rho)$ initially vanishes at the boundary of the support, then a *waiting time* phenomenon occurs, where the edges of the support start moving at a positive time. Indeed, for initial data where the right-most point is given by $x_*(0)$, such that $\rho(x_*(0)-) > 1$ and $\rho(x_*(0)+) = 1$, we can calculate under consideration $f(1/\rho) = (\rho - 1)_+^m$ similar to (15) the velocity of the jump location

$$\dot{x}_*(t) = m\Big(\rho(x_*(t)-, t) - 1\Big)^{m-2} \partial_x \rho(x, t)_{|_{x=x_*(t)-}} .$$

One can see clearly that the smaller the exponent m and the closer the left-sided limit $\rho_0(x_*(0)-)$ is to the value 1, the flatter has to be the initial density ρ_0 left of the boundary point $x_*(0)$ in order to observe the aforementioned waiting time phenomenon.

Less clear is the situation with initial data of the form $\rho_0(x) = 1 - cx$, $c > 0$ and a general nonlinearity f. We conjecture that, on the one hand, a discontinuity develops with infinite initial speed as above, whenever $x = o(\partial_x f(1/\rho))$ as $x \to 0-$, and on the other hand, the discontinuity only appears after a waiting time for $\partial_x f(1/\rho) = o(x)$ as $x \to 0-$. However, we are not aware of any rigorous results on these questions.

Decay to equilibrium: The dynamics of (13) dissipates the L^2-norm. After continuation of ρ by zero outside of $[X_0, X_1]$, we obtain

$$\frac{d}{dt} \int_{\mathbb{R}} \rho^2 dx = 2 \int_{\mathbb{R}} \frac{1}{\rho^2} f'\left(\frac{1}{\rho}\right) (\partial_x \rho)^2 dx \le 0 .$$

The dissipation vanishes for $\rho < 1$ or ρ independent from x. During the evolution we expect to see intervals $I_+(t)$, where $\rho \ge 1$, separated from intervals $I_-(t)$, where $\rho < 1$, by moving jump discontinuities, where $\rho = 1$ are the boundary conditions for the intervals I_+. Therefore we expect that equilibria have intervals $I_{+,\infty}$, where $\rho \equiv 1$, separated by intervals $I_{-,\infty}$, where $\rho < 1$ and otherwise arbitrary. The number of $I_{+,\infty}$-intervals might be smaller than that of $I_+(0)$-intervals, since these intervals might merge by collisions of the moving jump discontinuities. As soon as this coarsening process is over, the limit $I_{+,\infty} = [a, b]$ of each interval $I_+(t)$ can be predicted. Let $[c, d]$ be big enough to contain $[a, b]$ with $\rho(c, t) = \rho_0(c), \rho(d, t) = \rho_0(d) < 1$. Then a and b can be computed from the conservation of mass and of the center of mass:

$$\int_c^d \rho_0 dx = b - a + \int_{[c,d]\setminus[a,b]} \rho_0 dx \quad \Longrightarrow \quad b - a - \int_a^b \rho_0 dx = 0 , \tag{16}$$

$$\int_c^d x\rho_0 dx = \frac{b^2 - a^2}{2} + \int_{[c,d]\setminus[a,b]} x\rho_0 dx \quad \Longrightarrow \quad \frac{b^2 - a^2}{2} - \int_a^b x\rho_0 dx = 0 . \tag{17}$$

4. The rigorous macroscopic limit

The macroscopic limit will be carried out in the individual based model in terms of the unknowns ω_i, as in (5). However, boundary conditions will be avoided by considering a countable number of particles distributed over the whole real axis. Therefore we consider the initial value problem

$$\begin{aligned} \dot{\omega}_i &= -\frac{f(\omega_{i-1}) + f(\omega_{i+1}) - 2f(\omega_i)}{\Delta s^2} , \\ \omega_i(0) &= \omega_{i,0} , \qquad i \in \mathbb{Z} , \end{aligned} \tag{18}$$

with initial data satisfying

$$0 \le \omega_{\min} := \inf_{i\in\mathbb{Z}} \omega_{i,0}\,, \qquad \sup_{i\in\mathbb{Z}} \omega_{i,0} =: \omega_{\max} < \infty\,. \tag{19}$$

Note that under the assumption (1) on the nonlinearity f the results of Theorem 1 remain valid, i.e. the existence and uniqueness of a global solution of (18), satisfying

$$\omega_{\min} \le \omega_i(t) \le \omega_{\max}\,, \qquad i \in \mathbb{Z}\,, \quad t \ge 0\,.$$

The connection to the continuum is made by the definition of the piecewise constant interpolant

$$\omega_{\Delta s}(s,t) := \omega_i(t) \qquad \text{for } (i-1/2)\Delta s \le s < (i+1/2)\Delta s\,, \quad t \ge 0\,. \tag{20}$$

The uniform bound already provides weak convergence (of an appropriate subsequence) as $\Delta s \to 0$, which is however not sufficient for passing to the limit in the nonlinearity. Therefore we additionally assume a uniform bound on the total variation of the initial data, which we enforce by assuming a finite number of changes of monotonicity. More precisely, with $\Delta\omega_i(t) := \omega_{i+1}(t) - \omega_i(t)$, $i \in \mathbb{Z}$, we consider sets of indices

$$i_1 < \ldots < i_K \quad \text{such that} \quad \Delta\omega_{i_k}(t)\Delta\omega_{i_{k-1}}(t) < 0\,, \quad k = 2, \ldots, K\,,$$

and denote by $M(t) \in \mathbb{N} \cup \{\infty\}$ the maximum of all such K. The additional assumption on the initial data is

$$M(0) < \infty\,. \tag{21}$$

With (19) this immediately implies a bound of the total variation:

$$TV(\omega_{\Delta s}(\cdot,0)) = \sum_{i\in\mathbb{Z}} |\omega_{i+1,0} - \omega_{i,0}| \le M(0)(\omega_{\max} - \omega_{\min})\,.$$

Lemma 3. *Let $(\omega_i,\, i \in \mathbb{Z})$ be a solution of (18). Then $M(t)$ as defined above is non-increasing.*

Proof. A change of the monotonicity behavior at time t requires the existence of an index i such that $\Delta\omega_i(t) = 0$. Additionally $\Delta\omega_{i-1}(t)\Delta\omega_{i+1}(t) \ge 0$ is necessary, i.e. there is monotonicity of the sequence $\omega_{i-1}(t), \ldots, \omega_{i+2}(t)$ of 4 points. Otherwise, i.e. for $\Delta\omega_{i-1}(t)\Delta\omega_{i+1}(t) < 0$, there is one local extremum at $\omega_i(t) = \omega_{i+1}(t)$, and this will be preserved at least for short time.

Thus, w.l.o.g. we assume

$$\omega_{i-1}(t) \le \omega_i(t) = \omega_{i+1}(t) \le \omega_{i+2}(t)\,.$$

This implies

$$\frac{d}{dt}(\omega_{i+1} - \omega_i)(t) = \frac{f(\omega_{i-1}(t)) - f(\omega_{i+2}(t))}{\Delta s^2} \ge 0\,,$$

by the monotonicity of f. Therefore the monotonicity of the 4 points is preserved and no additional extremum can be created. □

Actually the total variation could be expected to be non-increasing with time, but for our purposes the consequence

$$TV(\omega_{\Delta s}(\cdot,t)) \le M(t)(\omega_{\max} - \omega_{\min}) \le M(0)(\omega_{\max} - \omega_{\min})\,, \qquad t \ge 0\,, \tag{22}$$

of the lemma will be sufficient. It provides a bound on $\omega_{\Delta s} \in L^\infty((0,\infty); BV(\mathbb{R}))$ uniformly in $\Delta s > 0$. Moreover, the TV-bound can be used to also get some regularity in time.

Lemma 4. *With the assumptions of Lemma 3, $\partial_t\omega_{\Delta s} \in L^\infty((0,\infty); W^{1,-\infty}(\mathbb{R}))$ uniformly in $\Delta s > 0$.*

Proof. Considering a test function $\varphi \in W^{1,\infty}(\mathbb{R})$, we define

$$\varphi_i := \frac{1}{\Delta s}\int_{(i-1/2)\Delta s}^{(i+1/2)\Delta s} \varphi \, ds\,, \qquad J_i(t) := \frac{f(\omega_i(t)) - f(\omega_{i-1}(t))}{\Delta s}\,, \tag{23}$$

and compute

$$\int_{\mathbb{R}} \partial_t \omega_{\Delta s}\varphi \, ds = \sum_{i\in\mathbb{Z}} \dot\omega_i \varphi_i \Delta s = -\sum_{i\in\mathbb{Z}} \frac{J_{i+1}-J_i}{\Delta s}\varphi_i \Delta s = \sum_{i\in\mathbb{Z}} J_i \frac{\varphi_i - \varphi_{i-1}}{\Delta s}\Delta s$$

This leads to the estimate

$$\begin{aligned}\left|\int_{\mathbb{R}} \partial_t \omega_{\Delta s}(s,t)\varphi(s)\, ds\right| &\le \|\varphi'\|_{L^\infty(\mathbb{R})} \sum_{i\in\mathbb{Z}} |f(\omega_i(t)) - f(\omega_{i-1}(t))| \\ &\le \|\varphi'\|_{L^\infty(\mathbb{R})} M(0)(\omega_{\max} - \omega_{\min})\,, \qquad t \ge 0\,,\end{aligned}$$

where we have used the Lipschitz continuity of f and (22). □

As a consequence of our results, for a bounded interval $\Omega \subset \mathbb{R}$ we have

$$\omega_{\Delta s} \in L^\infty((0,\infty); BV(\Omega)) \qquad \text{and} \qquad \partial_t \omega_{\Delta s} \in L^\infty((0,\infty); W^{1,-\infty}(\Omega))\,.$$

Since, for $1 \le q < \infty$, $BV(\Omega) \subset L^q(\Omega) \subset W^{-1,\infty}(\Omega)$, where the first inclusion is compact [25, Corollary 3.49], we conclude from [37] that $\{\omega_{\Delta s}, \Delta s > 0\}$ is relatively compact in $L^p_{loc}((0,\infty)\times\mathbb{R})$ for every $p < \infty$.

For a test function $\varphi \in C_0^\infty([0,\infty)\times\mathbb{R})$ we test (18) against $\varphi_i(t)$, defined as in (23). After an integration by parts with respect to $t \ge 0$ and summation by parts with respect to $i \in \mathbb{Z}$ we obtain

$$\begin{aligned}&\int_{\mathbb{R}} \omega_{\Delta s}(s,0)\varphi(s,0) ds + \int_0^\infty \int_{\mathbb{R}} \omega_{\Delta s}\partial_t\varphi \, ds\, dt \\ &= \int_0^\infty \sum_{i\in\mathbb{Z}} f(\omega_i) \frac{\varphi_{i+1} - 2\varphi_i + \varphi_{i-1}}{\Delta s^2}\Delta s\, dt = \int_0^\infty \int_{\mathbb{R}} f(\omega_{\Delta s})\partial_s^2\varphi \, ds\, dt + O(\Delta s)\,,\end{aligned} \tag{24}$$

where the last equation follows from

$$\frac{\varphi_{i+1} - 2\varphi_i + \varphi_{i-1}}{\Delta s^2} = \frac{1}{\Delta s}\int_{(i-1/2)\Delta s}^{(i+1/2)\Delta s} \partial_s^2\varphi \, ds + O(\Delta s)\,.$$

Restricting to appropriate subsequences we have $\omega_{\Delta s} \to \omega$ in $L^p_{loc}((0,\infty)\times\mathbb{R})$ as $\Delta s \to 0$, and we may pass to the limit in (24):

$$\int_{\mathbb{R}} \omega_0(s)\varphi(s,0) ds + \int_0^\infty \int_{\mathbb{R}} \omega\partial_t\varphi \, ds\, dt = \int_0^\infty \int_{\mathbb{R}} f(\omega)\partial_s^2\varphi \, ds\, dt\,, \tag{25}$$

where $\omega_0(s)$ is the limit of the initial data $\omega_{\Delta s}(s,0)$, which exists by the BV-assumption (21). This is the weak formulation of the initial value problem

$$\partial_t \omega = -\partial_s^2 f(\omega)\,, \quad \text{in } (0,\infty)\times\mathbb{R}\,, \qquad \omega(s,0) = \omega_0(s)\,, \quad s \in \mathbb{R}\,. \tag{26}$$

Theorem 5. *Let (1), (19), and (21) hold. Let $\omega_{\Delta s}$ be defined by (20) in terms of the solution of (18). Then $\lim_{\Delta s\to 0}\omega_{\Delta s} = \omega$ in $L^p((0,\infty)\times\mathbb{R})$ for any $1 \le p < \infty$, restricting to appropriate subsequences. The limit $\omega \in L^\infty((0,\infty)\times\mathbb{R})$ is a weak solution of (26).*

Remark 6. An existence theory for the continuous problem written in terms of $x(s,t)$ (see (11)) can also be carried out by interpreting the problem as gradient flow for the energy functional

$$E[x] := -\int_{-\infty}^{\infty}\int_0^{\partial_s x} f(p)dp\, ds\,.$$

The basic theory (see e.g. [16]), however, only gives $x \in C([0,\infty); L^2(\mathbb{R}))$ and not much information on $\omega = \partial_s x$.

5. Numerical simulations

5.1. **Microscopic model:** We illustrate the previous statements with numerical experiments in x and ω. We solve the systems (3) and (5) for the choice

$$f(\cdot) := (1 - \cdot)_+ ,$$

with an implicit Euler algorithm to conserve the characteristic properties. We discretize as follows,

(27)
$$x_i^{n+1} = x_i^n + \frac{\Delta t}{\Delta s}\left[-\left(1 - \frac{x_{i+1}^{n+1} - x_i^{n+1}}{\Delta s}\right)_+ + \left(1 - \frac{x_i^{n+1} - x_{i-1}^{n+1}}{\Delta s}\right)_+ \right], \quad i \in \{1, \dots, N-1\},$$

including the boundary values x_0, x_N, based on classical ideas as in e.g. [7]. Also system (5) is treated similaraly.

We simulate $N = 20$ agents and chose a time-stepping of $\Delta t = 0.1\Delta s^2$ with $\Delta s = 0.1$ using a typical parabolic CFL-condition. The non-linearity f is solved with a fixed-point approach over $n = 40$ iterations as proposed in [23]. The results can be found in Figure 1.

The Min-Max-principle in Theorem 1 shows the relation with a parabolic system which has in general a smoothing effect, as can be seen in Figure 1b. However, this effect does not occur if the points x_i are too far apart, which is visualized in Figure 1c. Indeed, in that case groups of particles remain, which do not interact with each other. This fact will later motivate us to consider subproblems individually. Figure 1d visualizes the Min-Max-principle in Theorem 1, whereas also the time-dependent version stated Theorem 2 can be seen.

5.2. **Macroscopic model.** We investigate problem (13) on an open domain $\mathbb{R}$ with $\rho_0 > 0$ and discretize it as $\rho(i\Delta x, j\Delta t) = \rho_i^j$ explicit in time via

$$\rho_i^{j+1} = \rho_i^j + \frac{\Delta t}{\Delta x^3}\left[(1 - 1/\rho_{i+1}^j)_+ - 2(1 - 1/\rho_i^j)_+ + (1 - 1/\rho_{i-1}^j)_+\right]. \tag{28}$$

Here we discretized the Laplacian as usual.

We choose $\Delta x = 0.001$ for a sharp visualisation of the shock and $\Delta t = 0.1\Delta x^2$ in compliance with typical CFL-conditions, following classical literature, see [24]. In Figure (2a) we see the smoothing-effect for discontinuous initial data of system (13) for the spatial positions, where $\rho_0 > 1$.

In Figure 2b we furhter plot the position of the jump x_* calculated by (15). We used for the discretization of (15) an explicit Euler algorithm for solving the ODE. Knowing x_* is monotone increasing and considering the left- and right-handed limits, we used in the numerator a downwind- and for the denominator an upwind-approach. We see that the discretisation (28) creates the correct shock-speed. Additionally continuous initial data lead to satisfying results since as mentioned, the discontinuity only occurs for $t = 0$ and x_* is Lipschitz for $t > 0$.

In Figure 3 we visualized a simulation showing two colliding plateaus, i.e. two intervals, where the density ρ is greater than one, merge. The shocks move towards each other until the collision at time $t = 0.031$, where the two patches merge. The dynamics stop, once the final interval-length $[a, b]$ is reaches, where the boundaries a and b are calculated by (16)-(17).

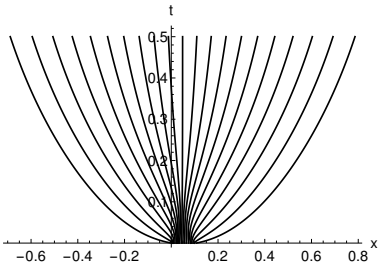

(A) The trajectories x_i over time, we see the agents moving away from each other. The initial values are chosen so that $x_i - x_{i+1} < \Delta s$ for all i, so all agents are in interaction.

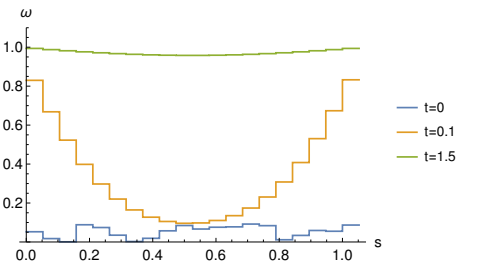

(B) The simulation associated with Figure 1a in ω, we see a smoothing effect with long term behavior $\omega_i \to 1$.

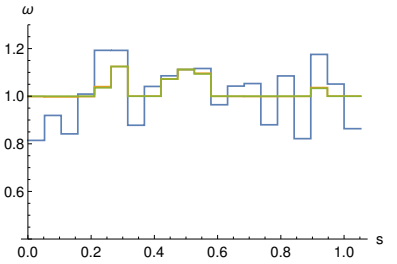

(C) Simulations in ω. The smoothing effect stops before all ω_i reach the value 1. This can be related to the fact that initially the threshold 1 is exceeded by a critical amount of ω_i, hence some plateaus will not interact since the points in between already reached the value 1.

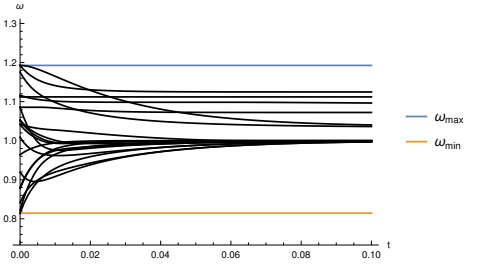

(D) The Min-Max-principle in Theorem 1 visualized for the dynamics associated to Figure 1c. Each black line corresponds to the time-evolution of a ω_i.

FIGURE 1. Time evolution of the discrete systems in ω and x for different initial values.

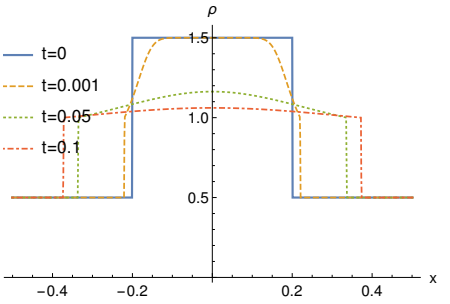

(A) Discontinuous initial data.

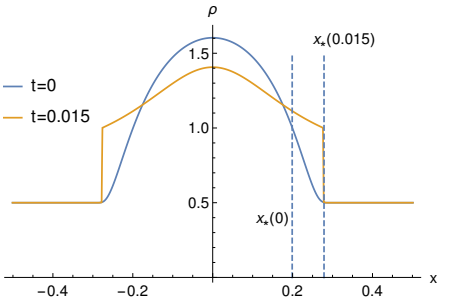

(B) Smooth initial-data and the position of the shock $x_\star$ calculated from (15).

FIGURE 2. Macroscopic simulations for two-sided problems.

5.3. **Comparison of the Microscopic and the Macroscopic Model.** We conclude the numerical simulations with an experiment, which compares the microscopic and the macroscopic dynamics in order to show consistency between the two scales. We start with

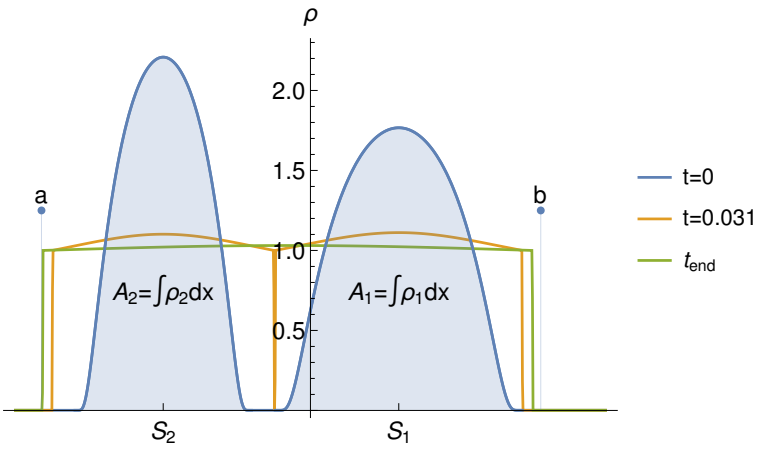

FIGURE 3. Two plateaus moving towards each other until they collide. The dynamics come to an end as soon the equilibrium size $[a, b]$ of the interval is reached.

a continuous initial density

$$\rho_0(x) := \begin{cases} 3\exp\left(\frac{0.09}{x^2-0.09}\right), & x \in (-0.3\,,0.3) \\ 0.5\,, & x \notin (-0.3\,,0.3) \end{cases}$$

and calculate the corresponding discrete values x_i via (12). In Figure 4 we see the solutions of the corresponding microscopic dynamics (5), solved numerically by (28), and the one of the corresponding macroscopic dynamics (13), solved via (27), which are plotted beside each other.

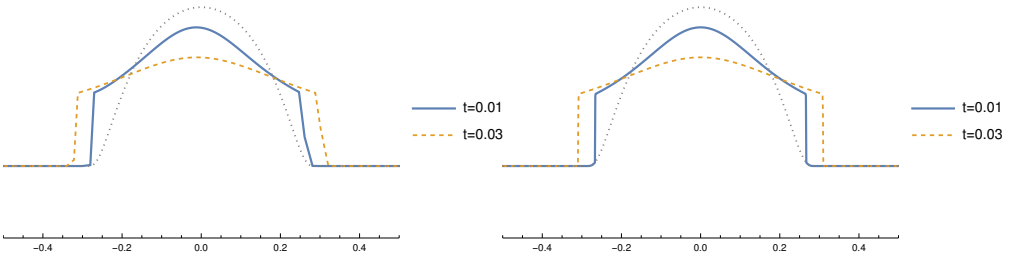

(A) Discontinuous initial data.

(B) Smooth initial-data and the position of the shock $x_\star$ calculated from (15).

FIGURE 4. Solution of microscopic system (28) and the macroscopic equation (**??**) showing the same dynamics.

6. Conclusion and Outlook

6.1. **Applications and open questions.** In the following, we mention two possible combinations for the new diffusion term $\partial_x^2\left(1-\frac{1}{\rho(x,t)}\right)_+$, which we obtain from our considerations above with the choice $f(\cdot) = (1-\cdot)_+$. The authors assume that both suggested models can presumably be derived microscopically.

Bacterial Growth. A classical growth term is exponential growth, which is well known to describe bacteria, see [28],

$$\partial_t \rho(x,t) = \rho(x,t).$$

This new diffusive effect needs to be investigated in the context of cell-exclusion, occurring in bacterial growth. This was done on a microscopic level by e.g. [14]. In a well known biological experiment, see [43], quite natural a version of a one-sided problem is investigated. Bacteria divide, and can leave a one-dimensional channel only on one side. The other has mathematically seen No-Flux boundary conditions. The experiment was done to investigate a growth-rate $\alpha > 0$. In our case, this corresponds to a one-sided problem with a source-term, e.g. in

$$\partial_t \rho(x,t) = \partial_x^2 \left(1 - \frac{1}{\rho(x,t)}\right)_+ + \alpha\rho(x,t).$$

From a mathematical perspective, questions regarding the existence of solutions and blow-ups are natural. The biological problem was investigated already with different technics, see [33], and this new diffusive term can broaden the perspective.

Alignments within a drift. We have shown how our diffusive term results in a desired density at the microscopic level. In addition, this term can be studied in systems with drift, for example, due to an external potential ϕ. If we motivate the drift term similar to a linear Fokker-Planck equation, it leads us to the following equation

$$\partial_t \rho(x,t) = \partial_x \left(\partial_x \left(1 - \frac{1}{\rho(x,t)}\right)_+ + \rho(x,t)\partial_x \phi(x) \right),$$

with ϕ being a suitable potential depending on x. This model has applications in 1D and 2D, see e.g. the self-organising system of birds during their travels.

The diffusion term D leads to a desired density ρ of 1, scaled here, but unlike macroscopic models based on cellular automata with cell exclusion, this can be exceeded and solve problems in modelling and calibration in the context of pedestrian dynamics, see [17, 19]. This new diffusion allows to introduce a parameter for the desired density ρ_d quite simply via

$$\partial_x^2 \left(1 - \frac{\rho_d}{\rho(x,t)}\right)_+ .$$

2D-setting. In the case of two or higher dimensions even the formal derivation of the macroscopic model is an open question. What makes the 1D case more solvable is the fact that one can define discrete gradients of the density in the following way

$$\rho_i := \frac{\Delta s}{x_{i+1} - x_i}.$$

Hence, an equidistant partition of the Lagrangian variable suggests the natural structure including the discrete gradient, while in higher dimensions the choice of the reference grid is non-unique and non-trivial. Nearby ideas of the authors is investigating the problem in 2D using e.g. Delaunay- and or Voroi-diagramms in combination with Lagrange-coordinates as in Figure 5. The latter are typical in measuring density in pedestrian dynamics, see [1], while the dual graph, the Delaunay-triangulation, see [30], can be used to define the interacting particles.

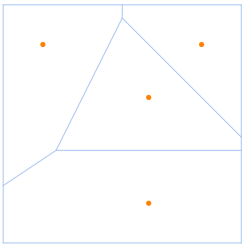

(A) Voronoi-diagram of random initial data in 2D.

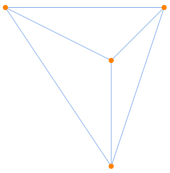

(B) Corresponding Delaunay-diagram, it is the dual graph.

FIGURE 5. The Voronoi-diagramms partitions the plane into sets s_i where x_i is the closest, while the Delaunay-diagram connects interacting particles based on the first.

6.2. **Summary and Conclusion.** In this work we modelled particles interacting in a certain radius. We introduce the scaled distance ω, which can also be seen as a derivative in Lagrangian coordinates s. From this interpretation, it was possible to define a microscopic density ρ by inverting ω.

For the microscopic systems (3) and (5) we could establishe an existence and uniqueness result, together with a maximum-principle (Theorem 1). This result as well as observations of the particle's positions (Theorem 2) are underlined with simulations in Section 5.1. Properties of (5) for x and ω can be transferred to the density ρ.

On a macroscopic level our main focus was on (13), a conservation law for which we could derive jump conditions for discontinuous initial data, which can be related to the moving boundary of a Stefan problem. Moreover, we discussed specific choices for the repulsive force f, which lead to well known nonlinear diffusion equations as the porous medium equation or the fast diffusion equation. A rigorous limit from (5) to (26) could be established. Due to the non-linearity f, passing to the limit is non-trivial. In order to conclude by finding a weakly convergent sequence for system (5), we used bounds on the total variation with respect to the spatial variable of the solution and a compact interpolation theorem [37].

Acknowledgments: We thank *Diane Peurichard* for fruitful discussions forming the starting point for these investigations.
This work has been supported by the Austrian Science Fund, grants no. W1245 and F65. L.K. received funding by the European Commission under the Horizon2020 research and innovation programme, Marie Sklodowska-Curie grant agreement No 101034255.

REFERENCES

[1] J. Adrian, M. Boltes, S. Holl, A. Sieben, and A. Seyfried. Crowding and queuing in entrance scenarios: influence of corridor width in front of bottlenecks. *arXiv preprint arXiv:1810.07424*, 2018. 1, 6.1

[2] D. Andreucci. Lecture notes on the stefan problem. *Lecture notes, Universitá da Roma La Sapienza, Italy*, 2004. 3

[3] S. Bartels. Total variation minimization with finite elements: convergence and iterative solution. *SIAM Journal on Numerical Analysis*, 50(3):1162–1180, 2012. 1

[4] A. Blanchet and P. Degond. Kinetic models for topological nearest-neighbor interactions. *Journal of Statistical Physics*, 169(5):929–950, 2017. 1

[5] F. Bolley, J. A. Cañizo, and J. A. Carrillo. Mean-field limit for the stochastic vicsek model. *Applied Mathematics Letters*, 25(3):339–343, 2012. 1
[6] M. Burger and J.-F. Pietschmann. Flow characteristics in a crowded transport model. *Nonlinearity*, 29(11):3528, 2016. 1
[7] J. C. Butcher. *Numerical methods for ordinary differential equations*. John Wiley & Sons, 2016. 5.1
[8] J. Carrillo and J. L. Vázquez. Fine asymptotics for fast diffusion equations. *Communications in Partial Differential Equations*, 28(5-6):1023–1056, 01 2003. 3
[9] J. A. Carrillo, M. Fornasier, J. Rosado, and G. Toscani. Asymptotic flocking dynamics for the kinetic cucker–smale model. *SIAM Journal on Mathematical Analysis*, 42(1):218–236, 2010. 1
[10] J. A. Carrillo, M. Fornasier, G. Toscani, and F. Vecil. *Particle, kinetic, and hydrodynamic models of swarming*, pages 297–336. Birkhäuser Boston, Boston, 2010. 1
[11] A. N. Ceretani, N. N. Salva, and D. A. Tarzia. An exact solution to a stefan problem with variable thermal conductivity and a robin boundary condition. *Nonlinear Analysis: Real World Applications*, 40:243–259, 2018. 1
[12] F. Cucker and S. Smale. Emergent behavior in flocks. *IEEE Transactions on Automatic Control*, 52(5):852–862, 2007. 1
[13] M. Di Francesco, S. Fagioli, and E. Radici. Deterministic particle approximation for nonlocal transport equations with nonlinear mobility. *Journal of Differential Equations*, 266(5):2830–2868, 2019. 1
[14] M. Doumic, S. Hecht, and D. Peurichard. A purely mechanical model with asymmetric features for early morphogenesis of rod-shaped bacteria micro-colony. *Mathematical biosciences and engineering : MBE*, 17 6:6873–6908, 2020. 1, 6.1
[15] M.-C. Duvernoy, T. Mora, M. Ardré, V. Croquette, D. Bensimon, C. Quilliet, J.-M. Ghigo, M. Balland, C. Beloin, S. Lecuyer, et al. Asymmetric adhesion of rod-shaped bacteria controls microcolony morphogenesis. *Nature communications*, 9(1):1–10, 2018. 1
[16] L. C. Evans. *Partial differential equations*. American Mathematical Society, Providence, R.I., 2010. 6
[17] M. Fischer, G. Jankowiak, and M.-T. Wolfram. Micro-and macroscopic modeling of crowding and pushing in corridors. *arXiv preprint arXiv:1911.10404*, 2019. 6.1
[18] F. Font. A one-phase stefan problem with size-dependent thermal conductivity. *Applied Mathematical Modelling*, 63:172–178, 2018. 1
[19] S. N. Gomes, A. M. Stuart, and M.-T. Wolfram. Parameter estimation for macroscopic pedestrian dynamics models from microscopic data. *SIAM Journal on Applied Mathematics*, 79(4):1475–1500, 2019. 1, 6.1
[20] J. Haskovec. Flocking dynamics and mean-field limit in the cucker–smale-type model with topological interactions. *Physica D: Nonlinear Phenomena*, 261:42–51, 2013. 1
[21] Q. Hong, M.-j. Lai, and J. Wang. The convergence of a numerical method for total variation flow. *Journal of Algorithms & Computational Technology*, 15:17483026211011323, 2021. 1
[22] A. Ihsan and J. Tuwankotta. Godunov method for stefan problems with neumann and robin type boundary condition using dimensionless enthalpy formulation. In *AIP Conference Proceedings*, volume 2296, page 020086. AIP Publishing LLC, 2020. 1
[23] C. T. Kelley. *Iterative methods for linear and nonlinear equations*. SIAM, 1995. 5.1
[24] R. J. LeVeque and R. J. Leveque. *Numerical methods for conservation laws*, volume 214. Springer, 1992. 5.2
[25] D. P. Luigi Ambrosio, Nicola Fusco. *Functions of bounded variation and free discontinuity problems*. Oxford Mathematical Monographs. Oxford University Press, USA, 2000. 4
[26] C. M. Mayr and G. Köster. Social distancing with the optimal steps model. *Collective Dynamics*, 6:1–24, Dec. 2021. 1
[27] A. M. Meirmanov. *The stefan problem*, volume 3. Walter de Gruyter, 2011. 1
[28] J. Monod. The growth of bacterial cultures. *Annual review of microbiology*, 3(1):371–394, 1949. 6.1
[29] S. Motsch and D. Peurichard. From short-range repulsion to hele-shaw problem in a model of tumor growth. *Journal of mathematical biology*, 76(1):205–234, 2018. 1
[30] O. R. Musin. Properties of the delaunay triangulation. In *Proceedings of the thirteenth annual symposium on Computational geometry*, pages 424–426, 1997. 6.1
[31] J. A. Perez. *Convergence of numerical schemes in the total variation sense*. New York University, 2004. 1
[32] R. Pinnau and C. Totzeck. Space mapping-based receding horizon control for stochastic interacting particle systems: dogs herding sheep, 2019. 1
[33] L. Robert, M. Hoffmann, N. Krell, S. Aymerich, J. Robert, and M. Doumic. Division in escherichia coliis triggered by a size-sensing rather than a timing mechanism. *BMC biology*, 12(1):1–10, 2014. 6.1
[34] L. Rubinstein. *The Stefan Problem*, volume 8. American Mathematical Soc., 2000. 1

[35] B. A. Schlake. *Mathematical models for particle transport: Crowded motion*. PhD thesis, Citeseer, 2011. 1

[36] M. J. Seitz and G. Köster. Natural discretization of pedestrian movement in continuous space. *Physical Review E*, 86(4):046108, 2012. 1

[37] J. Simon. Compact sets in the space $L^p(O,T;B)$. *Annali di Matematica pura ed applicata*, 146(1):65–96, 1986. 4, 6.2

[38] D. Tarwidi and S. Pudjaprasetya. Godunov method for stefan problems with enthalpy formulations. *East Asian Journal on Applied Mathematics*, 3:2013, 05 2013. 1

[39] A. Tveito. Convergence and stability of the lax-friedrichs scheme for a nonlinear parabolic polymer flooding problem. *Advances in Applied Mathematics*, 11(2):220–246, 1990. 1

[40] J. L. Vázquez. *Smoothing and Decay Estimates for Nonlinear Diffusion Equations: Equations of Porous Medium Type*. Oxford University Press, 1/11/2023 2006. 3

[41] J. L. Vazquez. *The Porous Medium Equation: Mathematical Theory*. Oxford University Press, 10 2006. 3

[42] T. Vicsek, A. Czirók, E. Ben-Jacob, I. Cohen, and O. Shochet. Novel type of phase transition in a system of self-driven particles. *Phys. Rev. Lett.*, 75:1226–1229, Aug 1995. 1

[43] P. Wang, L. Robert, J. Pelletier, W. L. Dang, F. Taddei, A. Wright, and S. Jun. Robust growth of escherichia coli. *Current biology*, 20(12):1099–1103, 2010. 6.1

[44] Z. You, D. J. Pearce, A. Sengupta, and L. Giomi. Geometry and mechanics of microdomains in growing bacterial colonies. *Physical Review X*, 8(3):031065, 2018. 1

M. Fischer: Universität Wien, Fakultät für Mathematik, Oskar-Morgenstern-Platz 1, 1090 Wien, Austria, & Universität Graz - Institut für Mathematik und Wissenschaftliches Rechnen, Harrachgasse 21, 8010 Wien, Austria, michi.fischer@univie.ac.at

L. Kanzler: CEREMADE, Université Paris Dauphine, Place du Maréchal de Lattre de Tassigny, F-75775 Paris Cedex 16, France, laura.kanzler@dauphine.psl.eu

C. Schmeiser: Universität Wien, Fakultät für Mathematik, Oskar-Morgenstern-Platz 1, 1090 Wien, Austria, christian.schmeiser@univie.ac.at